Available online at www.CivileJournal.org

Civil Engineering Journal

(E-ISSN: 2476-3055; ISSN: 2676-6957)

Vol. 11, No. 11, November, 2025

Shrinkage Characteristics and Abrasion Resistance of Porcelain Waste-Based Geopolymers Mortar Under Chemical Exposure

Rada Klingsad [1], Borvorn Israngkura Na Ayudhya [1*]

[2] *Department of Civil Engineering, Faculty of Engineering, Rajamangala University of Technology Thanyaburi, Pathum Thani 12110, Thailand.*

Received 02 May 2025; Revised 07 October 2025; Accepted 11 October 2025; Published 01 November 2025

Abstract

This study investigated microstructural analyses, dry shrinkage, and autogenous shrinkage of mortar using defective sanitary ware porcelain as a low-calcium material with sodium hydroxide (NaOH) and sodium silicate (Na_2SiO_3). Additionally, the abrasive resistance of concrete was examined under chemical corrosion environments of 5%, 10%, 15%, and 20% H_2SO_4, HCl, and $MgSO_4$. The microstructural analyses using XRF, DTA-TGA, and SEM were conducted at 28 days. For specimen preparation, mortar specimens were oven-cured for 2 h at 105°C, while concrete specimens were oven-cured for 24 h and air-cured for 28 days before undergoing chemical immersion at 3, 7, 14, 21, 28, 60, and 90 days. NaOH concentrations of 8, 10, 12, and 14 Molar (M) were used. The results indicated that shrinkage in porcelain-based geopolymer mortars increased with higher NaOH concentration, and increasing the initial curing temperature led to increased mortar shrinkage. The autogenous shrinkage of 14M alkali-activated porcelain mortar was found to be higher than that of 8M, 10M, and 12M NaOH concentration mortars. Additionally, increasing the NaOH concentration reduced the abrasive resistance of the concrete. The maximum weight loss values were 8.21%, 6.91%, and 0.96% for 20% H_2SO_4 (90 days immersion), HCl (90 days immersion), and 20% $MgSO_4$ (90 days immersion), respectively. The microstructural findings confirmed the formation of gel-intact phases, highlighting the importance of curing time and NaOH concentration in low-calcium binder material. This study emphasized the critical role of curing temperature in optimizing the mechanical and durability properties of defective sanitary ware porcelain-based geopolymer.

Keywords: Geopolymers; Porcelain; Drying Shrinkage; Curing Temperature.

1. Introduction

Porcelain sanitary ware production is highly energy-intensive and ranks among the highest energy consumers in the manufacturing sector. It accounts for approximately 30% of the total manufacturing process cost [1]. The energy sources typically include hydroelectric power, liquefied gas, and fossil fuel. A substantial amount of energy is required to reach and maintain the high temperatures necessary for baking and firing processes. During production, harmful emissions such as carbon monoxide (CO), carbon dioxide (CO_2), sulfur dioxide (SO_2), and heavy metals are released into the atmosphere. Defects and waste products are an unavoidable outcome of the manufacturing process. Discarded defective items are often disposed of in landfills, where they can release toxic chemical substances into the environment. Over a decade ago, an estimated 30% of daily production volume was classified as defective or waste material [2, 3]. However, recent advancements have significantly reduced waste in ceramic production lines, now accounting for only 3-7% of global output. Notably, 100% of raw waste can be reused in the dough preparation process, while fired waste is either sent to landfills (approximately 500,000 tons per year) or repurposed as aggregate in concrete mixtures [4]. Improper or unregulated landfill disposal poses risks of groundwater contamination. Reducing carbon dioxide emissions and minimizing resource consumption remain critical environmental concerns. Current sanitary ware production methods

* Corresponding author: borvorn_i@rmutt.ac.th

http://dx.doi.org/10.28991/CEJ-2025-011-11-012

also contribute to airborne nanoparticles, which are linked to respiratory illnesses. These fine particles circulate within the working environment and pose greater health risks than larger particulates. A shift toward more eco-friendly and cost-effective approaches in manufacturing and waste treatment could significantly mitigate the environmental impact. Given the hazards associated with toxic gas emissions and harmful substances released during production, stakeholders, including manufacturers, environment assessors, and researchers, are actively pursuing low-energy, low-emission alternatives to enhance sustainability in the industry.

Concrete is another construction material with a significant environmental footprint [5]. Cement, the most widely used conventional binding material, is responsible for approximately 7% of global greenhouse gas emissions [6]. Comparative environmental impact assessments of ceramic and concrete products have shown that ceramic materials are generally more sustainable than cement-based alternatives [7]. One effective strategy to reduce the environmental impact of defective outputs from both porcelain sanitary ware and cement production is the incorporation of waste materials into concrete structures. This approach promotes sustainability by repurposing industrial waste while maintaining acceptable mechanical and durability properties in the resulting products [8]. By utilizing controlled alkali concentrations, chemical activators, and calcium-based binder materials, researchers have developed eco-friendly alternatives to traditional cement. Geopolymers, in particular, are low-carbon cementitious binders formed through the activation of calcium-containing precursors with alkaline solutions. Their adoption offers a promising pathway toward reducing environmental impact and advancing sustainable construction practices.

Several studies have explored the use of ceramic and porcelain products in the production of alkali-activated binder (AAB) mortar and concrete. Coarse-ground electrical insulators, fired at temperatures above 1300 °C, have been used as replacements for natural aggregates [9]. Similarly, fine-ground electrical insulator powder has been partially blended with Portland cement [10]. Results indicate that substituting both coarse aggregates and fine powders enhances compressive and tensile strength. Porcelain sanitary ware products have also been investigated as replacements for coarse aggregates [11] and as fine binder materials. Studies have shown that the porosity and chloride ingress of porcelain-based geopolymer matrix mortar and concrete are reduced [12]. Porcelain stoneware has been successfully utilized as an alkali-activated material, achieving a compressive strength of 36 N/mm² when cured at 65 °C for 7 days. Additionally, porcelain tile polishing residue has been evaluated for its performance in AAB systems. When used as a 15% partial aluminosilicate replacement mixed with metakaolin, the resulting binder achieved a compressive strength of up to 72 N/mm² at 28 days [13]. Porcelain, being a low-calcium material, can serve as a cementitious precursor in the geopolymerization process. The combination of an alkaline activating solution and a solid aluminosilicate triggers a polymerization reaction that produces a binding matrix with enhanced mechanical properties, improved resistance to acid and sulfate attacks [14], and reduced matrix shrinkage [15].

Shrinkage mitigation in geopolymer concrete occurs through the reduction of capillary stresses, deceleration of reaction kinetics, and enhancement of pore structure via void filling. Porcelain waste exhibits a dense microstructure but limited chemical reactivity, which contributes to reduced shrinkage in geopolymer matrix. Alkali activation of porcelain waste typically involves solutions such as NaOH or KOH, initiating the dissolution of silicon (Si) and aluminum (Al), followed by polycondensation into N-A-S-H gel networks. Higher NaOH concentrations accelerate reaction kinetics but also increase early shrinkage due to rapid water consumption. Elevated curing temperatures enhance strength development; however, they also intensify drying shrinkage as a result of moisture loss. The dense and chemically inert nature of porcelain waste plays a critical role in shrinkage mitigation. By refining the pore network and reducing mesoporosity, it lowers capillary stresses—one of the primary drivers of drying shrinkage. Furthermore, its low chemical reactivity slows down geopolymerization kinetics, effectively buffering autogenous shrinkage during the early stages of hydration [16].

The hydration products of alkali-activated low-calcium precursor materials are relatively free from calcium-silicate-hydrate (C-S-H) and contain less expansive ettringite compared to high-calcium binding systems. Selecting an appropriate precursor can help reduce shrinkage-related damage [17]. Unlike ordinary Portland cement (OPC) binders, low-calcium binder materials typically do not exhibit autogenous shrinkage [18]. At early ages, the autogenous deformation behavior of geopolymer-based low-calcium binders is primarily influenced by the type of raw material used. In later stages, the silica content in the activator plays a dominant role in controlling autogenous shrinkage behavior [19]. This deformation is mainly driven by chemical shrinkage and the intrinsic evolution of the gel structure [20]. Additionally, the fineness of the binding material affects autogenous shrinkage by influencing the pore structure of alkali-activated binders. Finer pore structures increase the risk of shrinkage-related damage [21]. In cement-based materials, autogenous shrinkage is closely linked to chemical reactions, microstructure development and internal relative humidity [22]. Ridtirud et al. [23] investigated the effects of NaOH concentration, activator modulus, liquid-to-solid ratio, curing temperature and curing time on the shrinkage behavior of fly ash Type F. Their findings revealed that NaOH concentration and activator modulus have a relatively minor impact on drying shrinkage, whereas curing temperature and liquid-to-solid ratio are the predominant factors influencing shrinkage in fly ash-based geopolymers.

In low-calcium-based geopolymer paste, drying shrinkage is more significant than autogenous shrinkage and can lead to severe cracking [24, 25]. The granular distribution of aggregates and binder particles influences compactness, which directly affects drying shrinkage [26]. Olvera et al. [27] reported that ambient temperature, combined with a low alkali concentration (8 M), significantly influences the degree of shrinkage in geopolymer slurry specimens. Shrinkage in low-calcium fly ash slurry specimens progressively increases as the curing temperature rises to 50 °C, resulting in visible cracking. Geopolymer specimens experience higher internal stresses than ordinary Portland cement (OPC)

systems. However, at room temperature, low-calcium fly ash-based geopolymer slurry exhibits less shrinkage than OPC. A higher silica content and lower calcium concentration help minimize autogenous deformation and reduce drying shrinkage [28]. In alkali-activated slag systems, the rate of water loss is greater than in porcelain-based geopolymers, leading to more pronounced desiccation shrinkage [29]. As water migrates through the matrix, it generates high capillary pressures within the micropore network, which in turn initiates crack propagation in the microstructure [30, 31].

Steiner et al. [32] reported that incorporating ceramic polishing waste into alkali-activated matrices effectively delays the onset of autogenous shrinkage, thereby reducing total shrinkage. Conversely, Sun et al. [33] and Reig et al. [34] found that elevated curing temperatures do not significantly enhance the compressive strength of alkali-activated ceramic waste. Nonetheless, investigating the influence of high-temperature curing on the mechanical development of porcelain waste powder presents notable economic advantages. Further research is needed to understand the effects of porcelain waste on mortar shrinkage behavior and the durability of concrete exposed to chemical attack. Studies on alkali-activated porcelain waste as a cementitious material remain limited, primarily due to the labor-intensive preparation process, which involves crushing, cutting, grinding, and sieving. A key knowledge gap persists regarding the impact of porcelain waste on drying shrinkage in geopolymer systems derived from sanitary ware porcelain. Additionally, data on the chemical durability of porcelain-based geopolymer concrete under aggressive environmental conditions is scarce. Geopolymers, known for their highly mesoporous structure, typically exhibit greater drying shrinkage than ordinary Portland cement (OPC) systems [35].

However, finely ground sanitary ware porcelain may help mitigate early-stage shrinkage during geopolymerization. This study utilizes industrially defective sanitary ware porcelain as the primary precursor to develop porcelain-based geopolymers via alkali activation. The investigation focuses on evaluating fundamental mechanical properties, drying and autogenous shrinkage behavior, mass loss, and corrosion resistance of porcelain-based geopolymer concrete subjected to chemical immersion in H_2SO_4, HCl, and $MgSO_4$. Microstructural changes and hydration product evolution were analyzed using scanning electron microscopy (SEM) and X-ray fluorescence (XRF). This research highlights the practical potential of porcelain-based geopolymer mortars and promotes the sustainable reuse of defective sanitary ware products. The objective is to assess the drying and autogenous shrinkage of geopolymer mortars formulated with varying NaOH concentrations and initial oven-curing temperatures, alongside evaluating their chemical resistance under diverse acidic, sulfate, and chloride exposures. Figure 1 illustrates the experimental process flowchart. The experimental methods for evaluating the mortar and concrete properties of porcelain-based geopolymer specimens were divided into two parts: the first focused on studying drying and autogenous shrinkage of mortar specimens, while the second examined the chemical resistance of concrete specimens exposed to H_2SO_4, HCl, and $MgSO_4$ at concentrations of 5%, 10%, 15% and 20% over immersion periods of 3, 7, 14, 21, 28, 60, and 90 days.

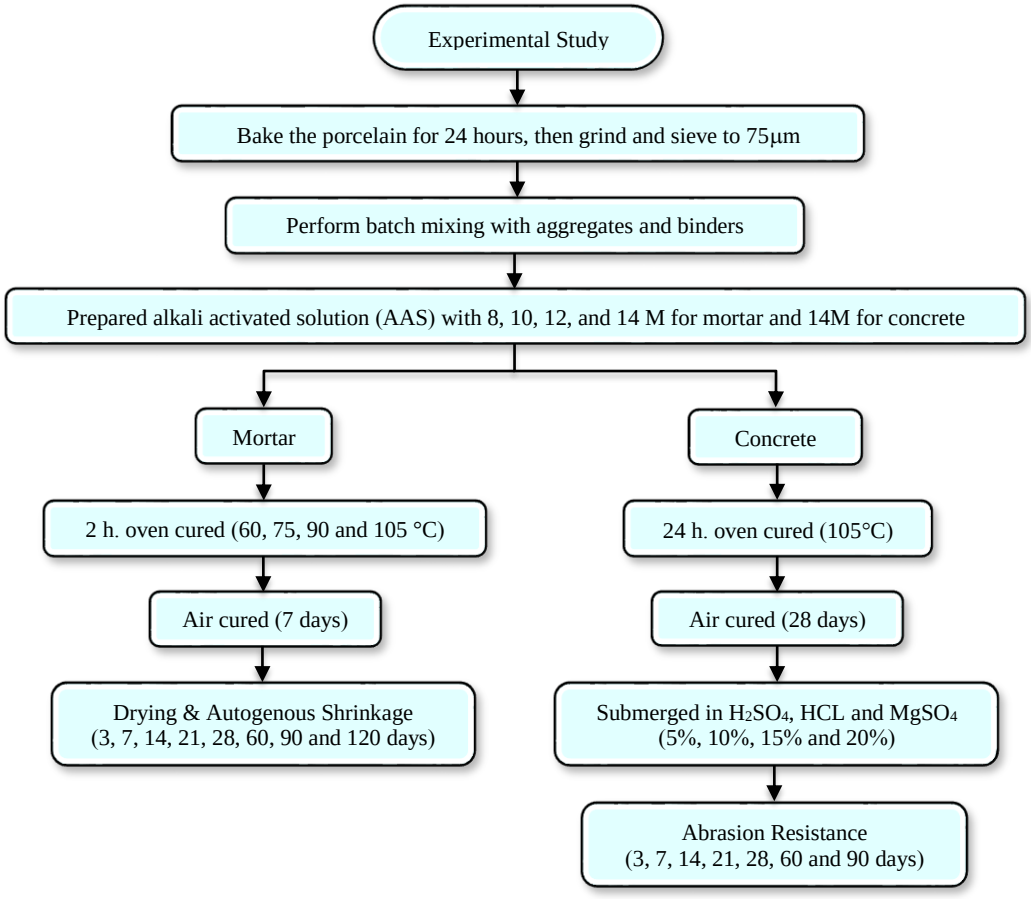

Figure 1. Experimental process

2. Materials

2.1. Cementitious Materials

Geopolymer material was prepared using defective sanitary ware products as the precursor, activated with a sodium silicate solution. The preparation of porcelain powder involved multiple mechanical stages to achieve a uniform particle size of less than 75 µm. As illustrated in Figure 2, the process included hammering large fragments of broken sanitary ware waste, grinding the coarse porcelain pieces, oven-drying, cutting with a rotating blade, and sieving to obtain a consistent porcelain powder. The oxide composition of the low-calcium material used in this study is presented in Table 1. X-ray fluorescence (XRF) analysis revealed that the porcelain waste primarily contained SiO_2 and Al_2O_3, at levels of 55.97% and 18.23% respectively. In contrast, the CaO content was relatively low, measured at 2.77%, indicating minimal calcium oxide presence in the porcelain waste. The X-ray fluorescence (XRF) analysis was performed using a Bruker S8 TIGER model under vacuum conditions to determine the elemental composition of the porcelain powder. Particle size distribution was analyzed using a laser diffraction particle size analyzer (Malvern Mastersizer 3000). The average particle sizes, represented by D50 and D90 values, were found to be 17.90 µm and 51.70 µm respectively.

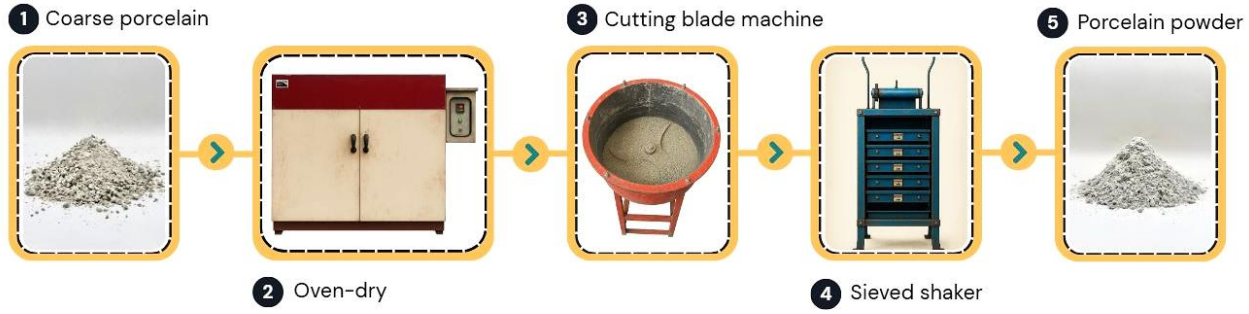

Figure 2. The granulation process of sanitary ware porcelain

Table 1. Oxides of defected sanitary porcelain

Oxides	Defected Sanitary Porcelain (%)
CaO	2.77
SiO_2	55.97
Al_2O_3	18.23
SO_3	0.02
Fe_2O_3	1.63
MgO	0.45
K_2O	3.08
TiO_2	0.22
Na_2O	1.13
Others	8.14
LOI	8.36
Particle size distribution	
Particle size	
D_{10}	2.01
D_{50}	17.9
D_{90}	51.7
Weight residual	0.86

2.2. Activating Solutions

Two different activator solutions were used: sodium hydroxide (NaOH) and sodium silicate (Na_2SiO_3). The alkali concentration was controlled at 8 M, 10 M, 12 M, and 14 M. The activating solutions were prepared by adjusting the appropriate amount of sodium silicate solution, followed by the addition of solid NaOH to achieve the desired modulus. The activator was first homogenized with deionized water, after which the precursor material was introduced. The activating solution was allowed to cool to room temperature for 24 hours before being mixed with ground porcelain to produce geopolymer mortar specimens. The prepared alkali activator solution and the weighed binder material were added to the mortar mixer pan and thoroughly blended.

2.3. Aggregates

The fine aggregate used in this study was land-based sand with a particle size smaller than 0.475 mm. Its specific gravity under saturated surface dry (SSD) conditions was measured at 2.66, and its water absorption was recorded at 0.24%. Additionally, the maximum size of coarse aggregate used in this study was 10 mm.

3. Experimental Methods

3.1. Mixture Preparation

Table 2 presented the mixture ratios of mortar and concrete specimens. In this study, superplasticizer was used to enhance mixture workability**.**

Table 2. Mixture proportion of mortar and concrete

Mortar									
Code	NaOH (M)	Solid content (%)	AAS Ratio	Materials (kg/m^3)					
				NaOH	Na_2SiO_3	Porcelain	Fine aggregate	SP	Curing temperature (°C)
GPC8	8	40.5	2.5	100	250	500	431.34	5	60,75, 90, 105
GPC10	10	44.5	2.5	100	250	500	431.34	5	60,75, 90, 105
GPC12	12	48.5	2.5	100	250	500	431.34	5	60,75, 90, 105
GPC14	14	52.5	2.5	100	250	500	431.34	5	60,75, 90, 105
Concrete									
Code	NaOH (M)	Solid content (%)	AAS Ratio	Materials (kg/m^3)					
				NaOH	Na_2SiO_3	Porcelain	Coarse aggregate	Fine aggregate	SP	Curing temperature (°C)
GPC14	14	52.5	2.5	100	250	500	1041.54	431.34	5	105

3.2. Specimen Preparation

3.2.1. Mortar

All geopolymer specimens were prepared using a standardized mixer pan, following established protocols at a mixing speed of 140 ± 5 rpm. Fine aggregates were added 30 seconds after mixing commenced]٣٦[. The test mortars were cast in two steps. First, the mortar was poured into pre-oiled steel molds measuring 25 × 25 × 280 mm, equipped with studs at both ends and a steel upper plate cover to prevent moisture loss and expansion. The specimens were vibrated for 10 seconds to ensure proper consolidation. All specimens were oven-dried for 2 hours to initiate the geopolymerization process, then allowed to cool at room temperature for an additional 2 hours before demolding. Each specimen was wrapped in polypropylene film and stored for seven days at 32 °C prior to testing. The designated testing ages were 3, 7, 14, 28, 60, and 90 days. For autogenous curing, specimens were wrapped with two layers of polypropylene film and two layers of aluminum foil to minimize moisture exchange and simulate sealed curing conditions.

3.2.2. Concrete

The mixing process for porcelain-based geopolymer concrete was similar to that of conventional concrete. Coarse and fine aggregates were mixed for 30 seconds using a mechanical mixer. Porcelain powder was then added and mixed for an additional 30 seconds to ensure uniform distribution. The dry mixture was thoroughly blended before adding sodium hydroxide (NaOH) and sodium silicate (Na_2SiO_3) solutions. These were mixed for 30 seconds, followed by the addition of a superplasticizer. The mixing process was completed by running the mixer for a further 90 seconds. For the preparation of hardened concrete specimens, cylindrical molds measuring 100 × 200 mm were used. The specimens were subjected to initial curing temperatures of 60 °C, 75 °C, 90 °C, and 105 °C for 24 hours. After curing, the specimens were cooled to room temperature and wrapped in polypropylene film for air curing over a period of 28 days. To evaluate chemical resistance, the cured specimens were submerged in H_2SO_4, HCl, and $MgSO_4$ solutions at concentrations of 5%, 10%, 15%, and 20%. Immersion durations were set at 3, 7, 14, 21, 28, 60, and 90 days.

3.3. Micro-Experimental Test Methods

The mortar specimens were crushed taken for different microscopic tests as follows*:*

- Scanning Electron Microscopy (SEM): A small specimen with a flat surface was vacuum-dried at 50°C for three days to prepare the SEM specimens. The Field Emission Scanning Electron Microscope and Energy Dispersive X-ray Spectrometer (FESEM-EDS, IT800SHL) were used to collect microscopic images under 500x and 2500x

- Simultaneous Thermal Analyzer (STA) Model NETZSCH STA 449F3 Jupiter was used to analyze the mass loss. The specimens were examined to track changes in weight during heating. The percentage of weight loss *(%* mass loss*)* was measured as the temperature increased to 1200°C at a heat rate of 10°C per minute under room temperature conditions. During testing process. The specimen's STA curve was automatically recorded.

3.4. Macro-Experimental Test Methods

Drying Shrinkage and Mass Loss

Figures 3-a and 3-b illustrate the prepared specimens for drying and autogenous shrinkage testing. The drying shrinkage test method employed in this study followed ASTM C157 standards [37]. A standard triple-connected drying shrinkage mold (25 × 25 × 280 mm) was used, equipped with holes at both ends for nail screws (6 × 25 mm). The mix ratio of cementitious material to fine aggregate was maintained at 1:1.16. After specimen preparation, all samples were cured in a standard curing room maintained at 32 ± 2 °C with a relative humidity of 85% until the designated testing dates. Measurements were conducted using a comparator equipped with a digital micrometer (accuracy: 0.001 mm) and a digital electronic balance (accuracy: 0.01 g). Prior to testing, the specimens were surface-cleaned, and their initial length (L_0) and initial mass (M_0) were recorded. At each testing age (3, 7, 14, 28, and 60 days), the specimens were measured for length (L_T) and mass (M_T). The drying shrinkage rate (S_T) and mass loss (m_L) at each age were calculated using Equations 1 and 2, respectively.

(a) Drying shrinkage specimens (b) Autogenous shrinkage specimens

Figure 3. Preparation of specimen for shrinkage test

$$S_T = \left(\frac{L_0 - L_T}{250}\right) \times 100\% \quad (1)$$

$$m_L = \left(\frac{M_0 - M_T}{M_0}\right) \times 100\% \quad (2)$$

Abrasive Resistance Test

An abrasion resistance test evaluates a material's ability to withstand wear and surface degradation. The results help predict the performance of a surface when subjected to friction against a moving counterpart. The test setup includes an abrasion device equipped with a rotating cutter, a precision balance, and a leveling plate. The apparatus consists of twenty-two dressing wheels, each with a diameter of 37.5 mm, mounted on washers that are stacked and secured onto a central bolt. The total cutter diameter is 82.5 mm. A normal load of 98 N is applied, with a testing frequency of three cycles lasting two minutes each [38]. During the test, the average mass loss (in grams) and abrasion duration are recorded. Mass loss is calculated using Equation 3, where m_0 represents the mass of the specimen before testing (mg), and m_a is the mass of the specimen after testing (mg).

$$\text{abrasion loss}\,(\%) = \left(\frac{m_a - m_o}{m_0}\right) \times 100\% \quad (3)$$

4. Results and Discussion

4.1. SEM

Figures 4-a to 4-f present SEM micrographs of porcelain-based geopolymer concrete specimens submerged in 20% concentrations of H_2SO_4, HCl, and $MgSO_4$, respectively. Specimens exposed to sulfuric acid solution for 90 days were compared with those immersed in hydrochloric acid and magnesium sulfate solutions. The micrographs revealed the presence of a few unreacted porcelain particles, along with visible voids and cracks in the matrix. The results indicate that using a high concentration of alkaline solution during geopolymer activation enhances the performance of porcelain-based geopolymerization. At 1,500× magnification, the surface of specimens exposed to sulfuric acid showed severe damage. Acid corrosion led to the deterioration of the microstructure, causing the fine aggregates to loosen and detach.

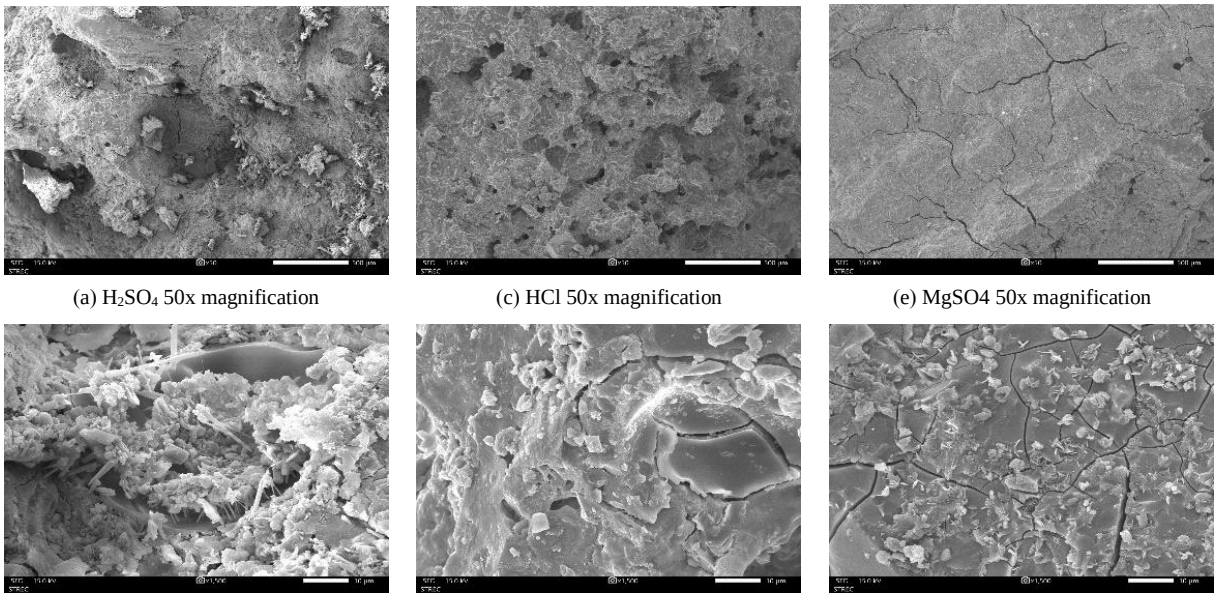

(a) H_2SO_4 50x magnification (c) HCl 50x magnification (e) MgSO4 50x magnification

(b) H_2SO_4 1500x magnification (d) HCl 1500x magnification (f) MgSO4 1500x magnification

Figure 4. SEM of specimen submerged in acidic and alkaline solutions

The deterioration of low-calcium-based geopolymer concrete was primarily attributed to the formation of zeolites and the depolymerization of geopolymeric products [39]. Morphological analysis of specimens attacked by sulfuric acid revealed gypsum as a corrosion product. The ingress of H_2SO_4 ions into the matrix led to the recrystallization of gypsum, which caused debonding of the aluminosilicate gel. However, due to the low calcium content in porcelain, the amount of gypsum formed was not significant. Interestingly, the presence of gypsum contributed to microstructural compaction and pore refinement, which helped reduce further sulfuric acid penetration into the matrix. As a result, the overall deterioration rate decreased [40]. The effects of hydrochloric acid exposure on porcelain-based geopolymer concrete at low magnification are shown in Figures 4-c and 4-d. Submerged specimens exhibited clear morphological signs of aluminum (Al) leaching, which led to increased porosity in the aluminosilicate gel. In Figure 4-c, several pores and voids were observed on the specimen surface, while Figure 4-d revealed crack formation. The leaching and disintegration of aluminosilicate contributed to cracking within the geopolymer matrix, weakening the surface integrity. However, the chemical transformation due to Al leaching was less pronounced in specimens exposed to H_2SO_4. No significant corrosion damage was observed in the matrix exposed to HCl, and it did not result in major strength deterioration. Overall, specimens exposed to H_2SO_4 exhibited more severe degradation than those exposed to HCl. Figures 4-e and 4-f show porcelain-based geopolymer concrete specimens submerged in $MgSO_4$ solution. Crystal precipitation and microcracking were observed on the specimen surfaces. The white precipitate was identified as magnesium sulfate hydrate, formed through the reaction of the solution with residual anions [41]. Excessive crystallization and precipitation of magnesium within the pores induced swelling stresses, leading to pore expansion. This process resulted in the formation of cracking lines and an increase in the total porosity of the specimens.

4.2. STA analysis

Figures 5 and 6 depict the temperature–mass loss behavior of porcelain-based geopolymer concrete specimens submerged in chemical solutions for 60 days, along with their corresponding TG/DTA curves. Across different chemical exposures, the mass loss patterns exhibited similar trends, with peak losses occurring within the temperature range of 25–1000 °C. This range was divided into six distinct decomposition stages: 25–100°C, 101–200°C, 201–400°C, 401–600 °C, 601–800 °C, and 801–1000 °C. For specimens exposed to H_2SO_4, mass loss during the first heating stage (25–100 °C) was primarily attributed to the evaporation of free water and partial dehydration of interlayer components [28, 42]. Specimens submerged in 20% H_2SO_4 solution exhibited rapid mass loss with increasing temperature, as shown in Figure 5. The mass loss rate was 0.12%/min, with an average total mass loss of 1.22%. In the second stage (101–200 °C), mass loss was mainly due to the release of chemically bonded water and decomposition of geopolymerization products. An endothermic peak was observed at a maximum temperature (T_{max}) of 152.8°C, corresponding to a mass loss of 6.59%. The mass loss rate during this stage was 0.77%/min, with an average mass loss of 6.25%, as presented in Table 3. When comparing DTA peaks in the first temperature range (25–100°C) across $MgSO_4$ and HCl matrices, Figure 6 shows that the peak for H_2SO_4 was higher than those for $MgSO_4$ and HCl. This behavior is attributed to the porcelain-based geopolymer concrete being less resistant to H_2SO_4 attack, resulting in lower density and higher porosity compared to specimens exposed to $MgSO_4$ and HCl [43]. In the third stage (201–400°C), the predominant contributor to mass loss was the decomposition of geopolymerization products. The slow release of chemically bound water resulted in a reduced mass loss rate, recorded at 0.53%/min, with an average mass loss of 9.67%. During the fourth stage (401–600°C), mass

loss was primarily attributed to the decomposition of calcite. A peak temperature of 530.7°C was observed, corresponding to a mass loss of 8.30%. The mass loss rate during this stage was 0.54%/min, with an average mass loss of 10.81%. The difference in mass loss between the first and second endothermic peaks was 4.33%. In the fifth stage (601–800°C), mass loss increased rapidly, with a rate of 0.60%/min and an average mass loss of 11.92%. During the sixth stage (801–1000°C), the specimen mass gradually decreased, with a mass loss rate of 0.68%/min. The third endothermic peak was recorded at 801.2°C.

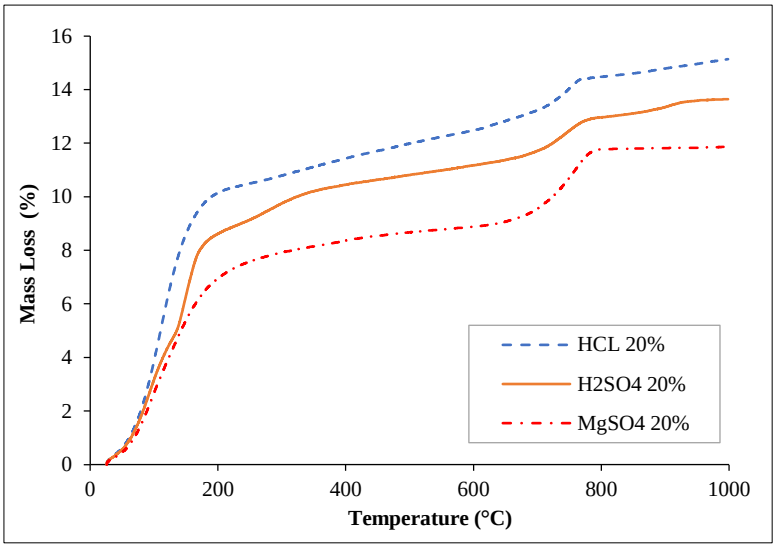

Figure 5. Mass loss of specimens submerged in acidic and alkaline solutions for 60 days

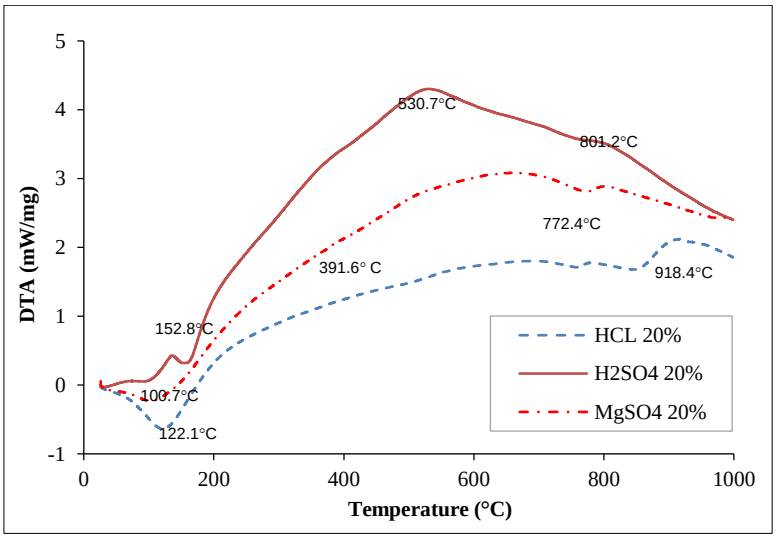

Figure 6. DTA of specimens submerged in acidic and alkaline solutions for 60 days

Table 3. Mass change over heating temperature of specimens submerged in acidic and alkaline for 60 days

Submerged solution	Mass change (%)					
Heating (°C)	25-100	101-200	201-400	401-600	601-800	801-1000
H_2SO_4	1.22	6.25	9.66	10.82	11.92	13.34
HCl	1.41	8.04	10.80	11.97	13.41	14.79
$MgSO_4$	1.01	5.21	7.85	8.66	9.92	11.83

Two distinct endothermic peaks were observed in the temperature ranges of 530–535 °C and 800–805 °C, corresponding to the dissociation of calcium and sulfate compounds with varying degrees of crystallinity. The difference in mass loss between the second and third peaks was calculated at 2.04%. For specimens submerged in HCl, the thermal curves exhibited endothermic peaks at 122.1 °C and 918.4 °C, which were associated with the evaporation of water from the material [44]. In the first stage, mass loss occurred rapidly at a rate of 0.02%/min, attributed to the removal of free water and the loss of physically adsorbed water in the aluminosilicate matrix [45].

In the second stage, the first endothermic peak appeared at approximately 122–124 °C, corresponding to a mass change of 9.07%. The mass loss rate during this stage was 0.08%/min, primarily due to dehydration of free water. In the third and fourth stages, mass loss gradually decreased compared to the second stage, with rates of 0.49%/min and 0.05%/min, respectively. In the fifth stage, mass loss continued to decline; however, between 760–775 °C, a slight increase in mass loss was observed. This was likely due to the decomposition of geopolymerization products and decarbonation of calcite [46], with a mass loss rate of 0.06%/min. In the sixth stage, the second endothermic peak appeared at 918–920°C, with a mass loss rate of 0.07%/min and a total mass change of 14.79%. This peak was primarily attributed to the loss of structured water, accompanied by the transformation of the material into a crystalline phase. The stabilization observed between 801–1000°C indicated that amorphous phases in HCl-submerged specimens were less prone to degradation at high temperatures compared to those exposed to H_2SO_4 and $MgSO_4$. This suggests that HCl-submerged specimens exhibited greater thermal stability. However, in terms of total mass loss, porcelain-based geopolymer concrete submerged in HCl experienced the highest loss compared to specimens exposed to H_2SO_4 and $MgSO_4$. This was due to the reaction of calcium-hydrated products with acids, forming calcium sulfate (gypsum), which precipitated on the specimen surface and led to the formation of a weak layer. The extent of weight loss was influenced by the stability of the geopolymer aluminosilicate structure [47]. In contrast, sulfuric acid exposure resulted in less mass loss than the HCl matrix.

For the $MgSO_4$ specimens, three distinct endothermic peaks were observed during thermal analysis between 25–1000 °C. In the first stage (below 100 °C), a sharp decrease in mass was recorded, primarily due to the dehydration of free water and the breakdown of C-A-S-H gel [48]. As the temperature increased, moisture continued to evaporate. Beyond 100 °C, chemically bound water within the structure was released at a rate of 0.014%/min, resulting in an average mass loss of 1.01%. The first endothermic peak appeared at 100.7 °C. In the second stage (101–200 °C), mass loss was attributed to the release of adsorbed water and water bound within the geopolymeric gel. The mass loss gradually increased, with a rate of 0.052%/min and an average loss of 5.21%. Thermal degradation occurred between 150–200 °C, specifically targeting the decomposition of N-A-S-H gel. During the third stage, mass loss decreased significantly compared to the second stage, with a rate of 0.04%/min. The second endothermic peak was observed at 391.6 °C, corresponding to an average mass loss of 8.32%. In the fourth stage (401–600 °C), mass loss continued at a steady rate of 0.04%/min, with an average loss of 8.66% (as shown in Table 3).

This phase involved dehydroxylation and the transition of geopolymerization products into a crystallized state. In the fifth stage (601–800 °C), the third endothermic peak appeared at 772.4 °C, corresponding to a mass loss of 11.41%. The mass loss rate was 0.05%/min. This stage marked the onset of sintering and further decomposition of the specimen. Notably, the specimens remained relatively stable beyond 700 °C, likely due to the low calcium content of porcelain, which limits the decomposition of calcium hydroxide at elevated temperatures. In the sixth stage (801–1000 °C), the mass loss rate increased slightly to 0.06%/min, with an average mass loss of 11.83%. This may be attributed to the polymerization reaction of free hydroxyl groups [49]. Overall, the total mass loss of $MgSO_4$-submerged specimens was lower than that of specimens exposed to HCl and H_2SO_4, indicating a higher retention of non-evaporated water in the $MgSO_4$ matrix.

Compared to low-calcium materials, thermograms of high-calcium systems such as slag-based geopolymers or ordinary Portland cement (OPC) exhibit distinct thermal behavior due to the presence of calcium-based hydrates. One of the most notable features is a pronounced endothermic peak associated with the decomposition of portlandite ($Ca(OH)_2$), typically observed between 450°C and 550°C. Additionally, a significant thermal event occurs above 500°C, corresponding to the breakdown of calcium silicate hydrate (C–S–H) gels, which are key contributors to strength development in high-calcium binders. Despite their initial mechanical advantages, high-calcium systems generally demonstrate lower overall thermal stability compared to low-calcium geopolymer systems. This reduced stability is attributed to the crystalline nature of calcium-based hydrates, which are more susceptible to thermal degradation. In contrast, low-calcium geopolymers often derived from materials such as fly ash or metakaolin form a predominantly amorphous aluminosilicate network. This structure remains more stable under elevated temperatures, offering superior resistance to thermal decomposition and making low-calcium geopolymers more suitable for high-temperature applications. These differences in thermal behavior underscore the importance of material selection based on intended service conditions, particularly in environments where thermal resistance is a critical performance factor.

4.3. Shrinkages

4.3.1. The Effect of Alkali Concentrations and Initial Curing Temperatures

To evaluate the effect of low-calcium binder components and initial curing temperature regimes on the shrinkage behavior of porcelain-based geopolymer mortar, specimens were subjected to both drying shrinkage and autogenous shrinkage tests. The drying shrinkage test was divided into two phases: early drying shrinkage and long-term (120-day) drying shrinkage. Early drying shrinkage was continuously monitored during the first 72 hours, while long-term shrinkage was evaluated at 3, 7, 14, 21, 28, 60, 90, and 120 days. Similarly, autogenous shrinkage was assessed through

early-stage measurements and 120-day evaluations. Curing temperature significantly influenced the properties of geopolymer materials. Figures 7 and 8 present the results of early shrinkage in porcelain-based geopolymer mortars oven-cured at 60°C, 75°C, 90°C, and 105°C for 2 hours. Among the four molar concentrations of NaOH (8 M, 10 M, 12 M, and 14 M), the 14 M specimens exhibited the most pronounced shrinkage response to initial curing temperature. The critical shrinkage period occurred between the 2nd and 60thh. At a curing temperature of 60°C, the average early drying shrinkage rate for 14 M specimens was 1.06 mm/m. At 75°C, 90°C and 105°C, the rates of drying shrinkage increased to 1.86, 1.94, and 2.18 mm/m respectively (Table 4). The highest early drying shrinkage rate was recorded at 40.8351 με/h during the 2nd h. Higher molar concentrations of alkali activator were associated with increased early drying shrinkage.

Elevated alkali levels accelerated the initial geopolymerization of porcelain, leading to rapid gel formation. This early gel formation hindered further geopolymerization reactions, increased porosity, and promoted early shrinkage [50]. Additionally, higher alkali equivalents intensified the geopolymerization process, enhancing the formation of reaction products that refined the pore structure and increased mesoporosity [51]. The refinement raised capillary pressure, contributing to greater drying shrinkage in porcelain-based geopolymer mortar specimens. Similarly, increasing the oven-curing temperature resulted in higher early drying shrinkage. The findings demonstrate a direct correlation between alkali concentration and drying shrinkage rates, consistent with the research of Peng et al. [52] and Lou et al. [53]. The higher degree of geopolymerization induced by elevated alkali concentrations promoted additional gel formation which reduced pore size and increased capillary shrinkage stress.

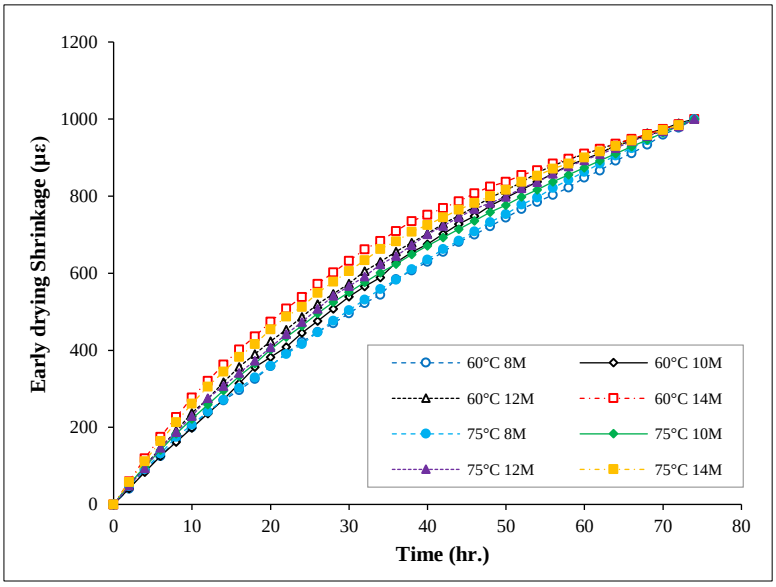

Figure 7. Early drying shrinkage at 60°C and 75°C curing temperature

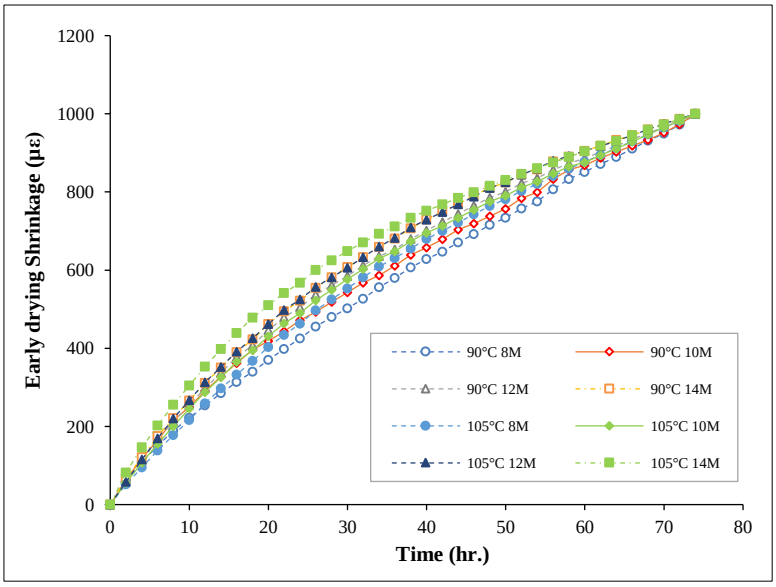

Figure 8. Early drying shrinkage at 90°C and 105°C curing temperature

Table 4. Early drying shrinkage of specimens (72 h)

Molar (M)	Total drying shrinkage (με)	Average shrinkage (mm/m)	Max. rate shrinkage (με/h)	Time of peak shrinkage (thh)
60°C				
8	780	0.78	20.9424	4
10	900	0.90	24.0740	4
12	955	0.96	25.4789	4
14	1064	1.06	29.9145	4
75°C				
8	1096	1.10	23.8680	2
10	1109	1.11	24.3523	2
12	1112	1.11	26.1375	2
14	1862	1.86	29.3009	2
90°C				
8	1151	1.15	28.6200	2
10	1328	1.33	30.7806	2
12	1710	1.71	32.1202	2
14	1944	1.94	33.6123	2
105°C				
8	1518	1.52	25.7800	2
10	1740	1.74	27.8100	2
12	1859	1.86	29.1603	2
14	2185	2.18	40.8351	2

The reduction in porosity resulting from higher activator concentrations contributed to lower final mass loss in the specimens. In contrast, specimens with lower activator concentrations exhibited larger pore structures and higher internal water content, allowing more free water to escape during curing. The drying shrinkage rate of mortars varied depending on both the alkali concentration and the initial curing temperature. Despite these variations, the overall patterns of early and long-term drying shrinkage in porcelain-based geopolymer mortar specimens remained broadly consistent across different curing conditions and activator levels. The results indicated that alkali-activated porcelain mortar subjected to initial curing temperatures exhibited thermal behavior similar to that of geopolymer concrete with low-calcium binders, such as fly ash type F (Figures 9 to12). A slight expansion of the specimens was observed, with the degree of expansion increasing proportionally with the curing temperature [54, 55]. Molar concentration was found to significantly influence the total drying shrinkage of alkali-activated porcelain mortar. The maximum drying shrinkage values are presented in Table 5. Specimens activated with higher molar concentrations of NaOH exhibited greater drying shrinkage, with the highest shrinkage observed in mortars produced using 14 M NaOH. In contrast, specimens activated with 8 M NaOH showed the lowest shrinkage values. The 14 M mortar also exhibited the highest rate of drying shrinkage, with peak shrinkage occurring between the 14th and 60th day. The average 120-day drying shrinkage rates for specimens oven-cured at 60 °C, 75 °C, 90 °C and 105 °C were 0.59, 0.93, 1.12 and 1.95 mm/m respectively. These trends were consistent with early drying shrinkage measurements. The results revealed a direct correlation between increased alkali concentration and higher drying shrinkage rates.

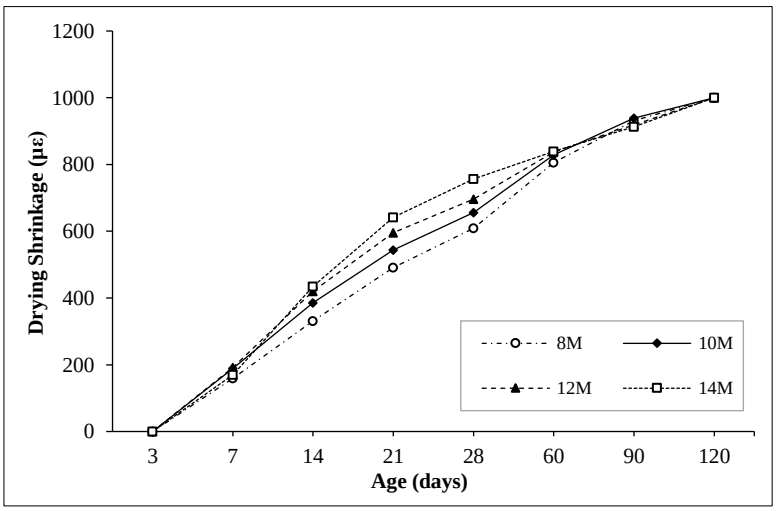

Figure 9. Drying shrinkage at 60°C curing temperature

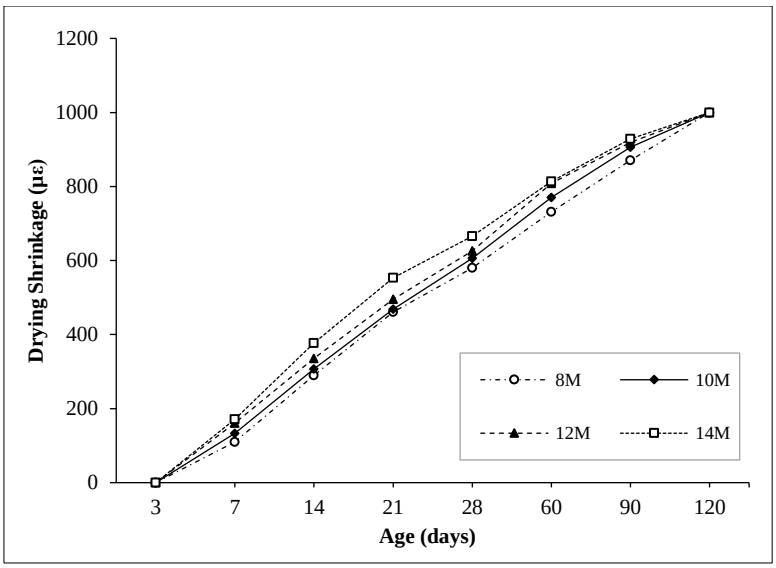

Figure 10. Drying shrinkage at 75°C curing temperature

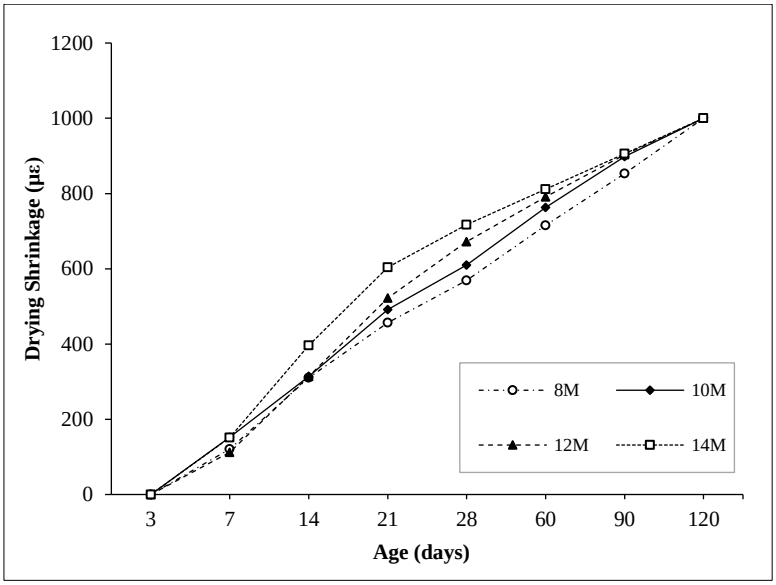

Figure 11. Drying shrinkage at 90°C curing temperature

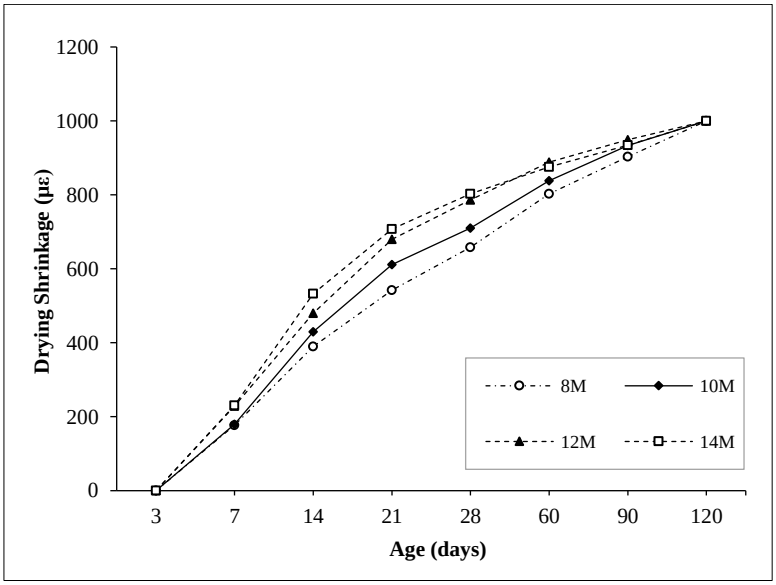

Figure 12. Drying shrinkage at 105°C curing temperature

Table 5. Drying and autogenous shrinkage of specimens (120 days)

Molar (M)	Total drying shrinkage (με)	Average shrinkage (mm/m)	Max. rate shrinkage (με/hr)	Peak shrinkage (thh)
		Drying shrinkage		
		60°C		
8	386.67	0.39	30.1724	7
10	446.67	0.45	29.8507	7
12	530.00	0.53	37.7358	7
14	590.00	0.59	38.1356	7
		75°C		
8	723.33	0.72	27.4399	7
10	891.27	0.89	42.8027	7
12	923.19	0.92	33.3988	7
14	933.46	0.93	40.1732	7
		90°C		
8	912.44	0.91	39.7557	7
10	1009.23	1.01	47.1239	7
12	1153.09	1.15	47.9970	7
14	1116.67	1.12	42.5373	7
		105°C		
8	1245.00	1.25	44.1767	7
10	1530.00	1.53	57.1895	7
12	1620.19	1.62	44.9471	7
14	1951.54	1.95	57.6906	7
		Autogenous shrinkage		
		60°C		
8	300.00	0.30	30.5556	7
10	463.33	0.46	32.3741	7
12	526.67	0.53	26.8987	7
14	1043.33	1.04	22.3642	7
		75°C		
8	320.00	0.32	31.2500	7
10	336.67	0.34	22.2772	7
12	440.00	0.44	30.3030	7
14	580.00	0.58	32.6050	7
		90°C		
8	323.33	0.32	44.3132	7
10	373.33	0.37	31.2500	7
12	376.67	0.38	42.0354	7
14	523.33	0.52	33.4395	7
		105°C		
8	465.00	0.47	34.9462	7
10	506.67	0.51	46.0526	7
12	605.00	0.61	39.2562	7
14	730.00	0.73	34.2466	7

Higher concentrations of alkali activator promoted the formation of a finer pore structure, which increased capillary stresses. As alkali concentration increased, aluminosilicate dissolution and depolymerization in the porcelain intensified, resulting in stronger alkali-metal cation binding within the matrix. This process reduced the presence of excess alkali-metal cations and other free ions, thereby enhancing the geopolymerization reaction and contributing to lower final mass

loss [56, 57]. In the case of ternary geopolymer concrete composed of slag, fly ash and ceramic waste powder, both porcelain-based geopolymer and ternary blended systems exhibited an increase in drying shrinkage during the early stages of curing which followed by stabilization over time. However, the porcelain geopolymer mortar demonstrated a significantly steeper initial shrinkage gradient compared to the slag–fly ash–ceramic waste blend. The ternary blended matrix recorded a drying shrinkage of approximately 348 µm at 28 days. This behavior suggests a heightened sensitivity to capillary moisture loss in porcelain-based systems. In contrast, the drying shrinkage of porcelain geopolymer mortar ranged from 569 to 803 µm, representing an increase of approximately 1.63 to 2.30 times relative to the ternary slag–fly ash–ceramic waste geopolymer concrete [58].

Autogenous shrinkage of porcelain-based geopolymer mortar was recorded after 24 hours of curing. The shrinkage primarily occurred within the first 24 hours, with values fluctuating within a narrow range. Measurements were recorded using scatter bars, and the characteristics of autogenous shrinkage are illustrated in Figures 12 and 13. The highest total autogenous shrinkage values for specimens activated with 8 M, 10 M, 12 M and 14 M NaOH concentrations were observed when specimens were oven-cured at 105 °C for 2 h. The corresponding shrinkage values were 465.00 µϵ, 506.67 µϵ, 605.00 µϵ, and 730.00 µϵ, respectively (Table 4). The maximum rates of autogenous shrinkage were 34.9462 µϵ/h, 46.0526 µϵ/h, 39.2562 µϵ/h, and 34.2466 µϵ/h respectively. A rapid increase in shrinkage rate was observed between the 3rd and 60th day of curing. The rate of autogenous shrinkage was found to increase with higher curing temperatures, as shown in Figures 13 and 14. Reported autogenous shrinkage values for geopolymer specimens typically range between 1400–3800 µϵ [59, 60]. Additionally, the peak time for both drying shrinkage and autogenous shrinkage was identified at the 7th h after mixing.

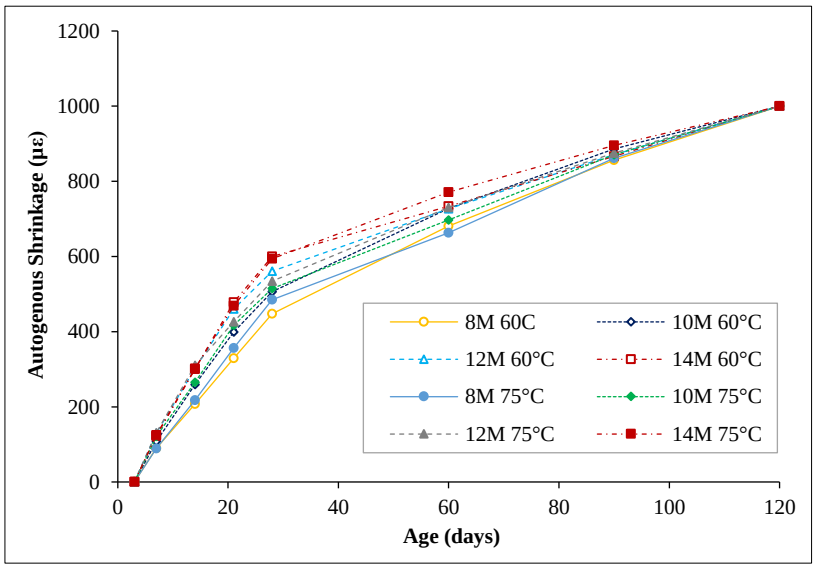

Figure 13. Autogenous shrinkage at 60°C and 75°C curing temperature

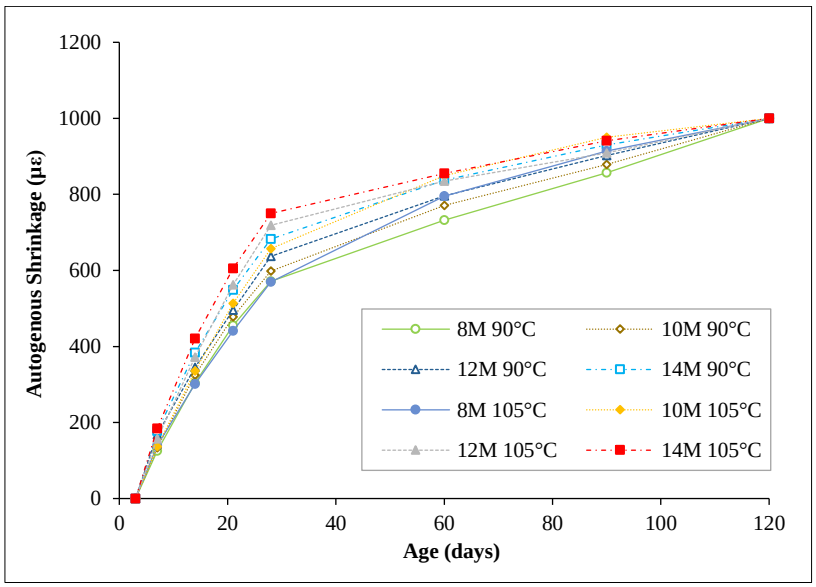

Figure 14. Autogenous shrinkage at 90°C and105°C curing temperature

Early drying shrinkage in porcelain-based geopolymer mortar was observed as early as the 2nd and 4th h after mixing. The trend in mass loss remained relatively consistent with the increase in drying shrinkage, indicating a strong correlation between moisture evaporation and dimensional change. Capillary water gradually migrated through the continuous micro-capillary pore network, resulting in significant shrinkage. Increasing the alkali dosage elevated capillary pore pressure within the specimens, intensifying self-desiccation and contributing to chemical shrinkage [61]. Consequently, higher sodium content was found to influence the shrinkage behavior of low-calcium binder systems. Similar shrinkage patterns have been reported in slag-based geopolymers [62, 63]. When compared to metakaolin, a commonly used low-calcium binder, porcelain-based geopolymers exhibited higher autogenous shrinkage. Metakaolin matrices typically show shrinkage values below 100 µm/m whereas porcelain-based specimens reached approximately 875 µm/m upon drying, closely aligning with the observed shrinkage magnitude [64].

An increase in sodium hydroxide (NaOH) concentration was found to intensify both early drying shrinkage and autogenous shrinkage in alkali-activated porcelain-based geopolymer concrete. The most pronounced shrinkage occurred at a NaOH concentration of 14 M, suggesting that higher alkalinity accelerates moisture loss and internal volume reduction. In contrast, the lowest shrinkage was recorded at 8 M, indicating that moderate alkali levels may help mitigate shrinkage-related issues. Peak shrinkage, both drying and autogenous was observed approximately 7 h after mixing, marking a critical period in the early curing phase. Notably, early drying shrinkage began to manifest as early as the 2nd and 4th h, underscoring the sensitivity of the mix to moisture loss shortly after casting. These findings highlight the importance of optimizing alkali concentration to balance activation efficiency with dimensional stability, particularly in porcelain-based geopolymer systems where shrinkage can significantly impact long-term durability and structural performance.

4.4. Abrasive Resistance

4.4.1. The Effect of Submerged Concentration

The specimens were immersed in acidic, chloride and sulfate for 3, 7, 14, 21, 28, 60 and 90 days. Before immersion, specimens were air-cured for 28 days. The exposure in chemical solution of porcelain based geopolymer concrete is one of the techniques to analysis durability pertaining to estimate long-term deterioration under chemical environments. Figures 15 and 16 illustrated the acid, sulfate and chloride resistance of porcelain based geopolymer specimens in terms of residual abrasive resistance strength after exposure to 5%, 10%, 15% and 20% concentration of H_2SO_4, HCl and $MgSO_4$ solutions. At early ages (3 and 7 days of immersion) strength of porcelain based geopolymer concrete was high. However, the percentage of weight loss from abrasive increased as the chemical immersion concentration increased. The rate of deterioration in abrasive resistance of H_2SO_4 and $MgSO_4$ gradually increased early age of immersion. The rate of deterioration begun to decline after 28 days toward 90 days of immersion. Among the three solutions, the rate of deterioration of H_2SO_4 was highest, followed by $MgSO_4$ and HCl respectively.

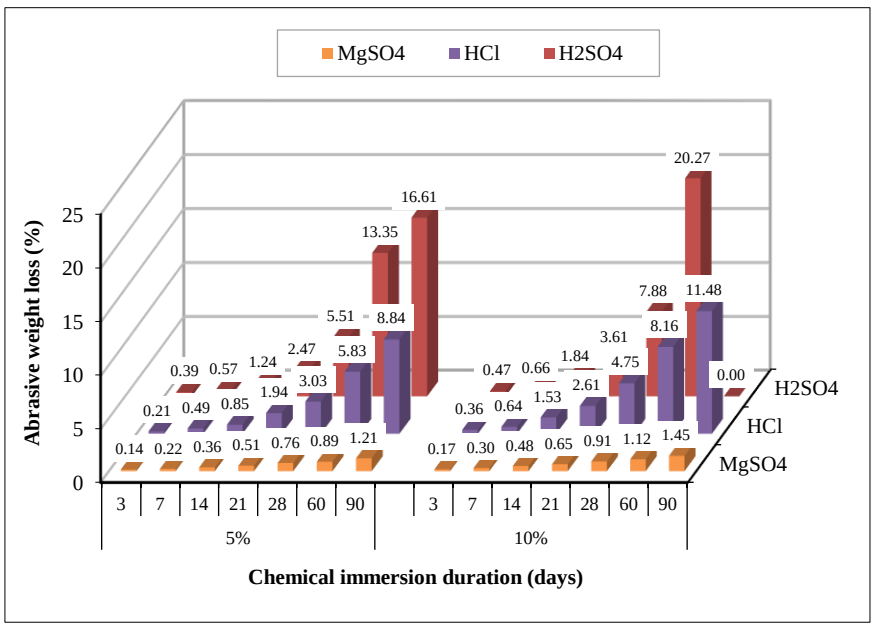

Figure 15. Abrasive resistance of specimens at 5% and 10% immersion

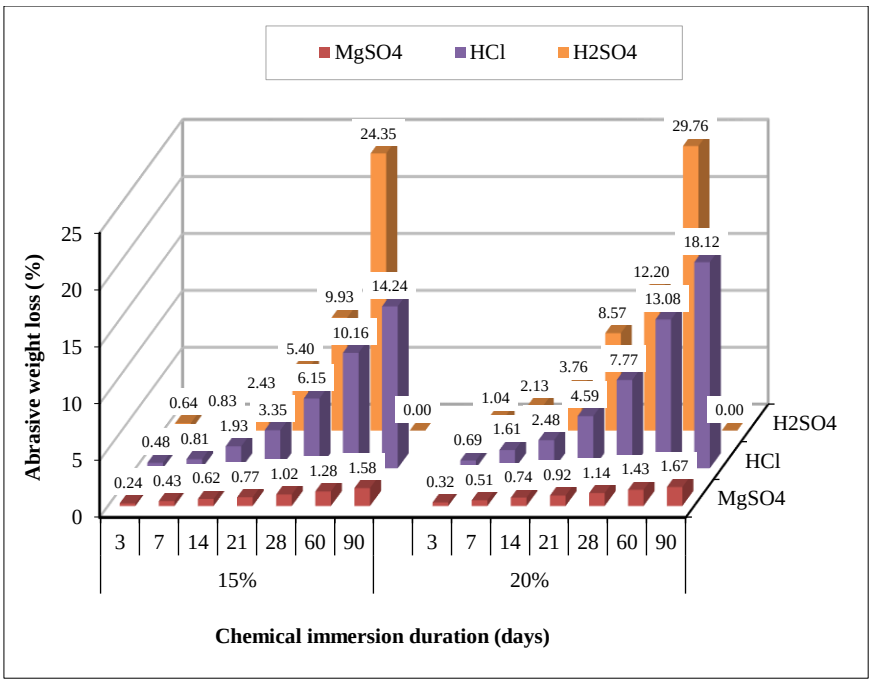

Figure 16. Abrasive resistance of specimens at 15 % and 20% immersion

At 14 and 21 days of immersion, a continued decrease in abrasive resistance was observed despite moderate curing durations. This trend suggests that strength deterioration was influenced by progressive microstructural degradation over time. The deterioration was closely linked to the calcium content of the binder material and the formation of calcium–(aluminum)–silicate–hydrate (C–(A)–S–H) gels resulting from the geopolymerization process [65, 66]. Table 6 presents the average percentage drop in weight loss from abrasion across immersion concentrations of 5%, 10%, 15%, and 20%. Experimental results indicated that early-age abrasive resistance values remained within acceptable limits for construction applications. By 60 days, the rate of weight loss had significantly declined. At 90 days under 20% chemical immersion, the daily weight loss rates for specimens exposed to H_2SO_4, HCl, and $MgSO_4$ were 0.181%, 0.168% and 0.008%, respectively. Overall, porcelain-based geopolymer specimens submerged in H_2SO_4 exhibited the highest cumulative weight loss, followed by HCl and $MgSO_4$. At 5% concentration, the total weight loss was 5.74% (H_2SO_4), 3.03% (HCl) and 0.58% ($MgSO_4$). At 20% concentration, the losses increased to 8.21%, 6.91%, and 0.96%, respectively. These results suggest that porcelain-based geopolymer concrete demonstrated greater durability when exposed to HCl compared to $MgSO_4$ and H_2SO_4. Following exposure to H_2SO_4 and HCl, specimens exhibited surface texture degradation and loss of orientation due to leaching and gypsum deposition. Salt precipitation became increasingly visible with higher solution concentrations.

The disintegration process was marked by both weight loss and surface salt accumulation. Previous studies have shown that the compressive strength of porcelain- and metakaolin-based geopolymer concrete [12], activated with sodium hydroxide and water glass, tends to increase as the Na_2O/SiO_2 molar ratio decreases [67]. Similarly, in fly ash-based and self-compacting geopolymer concrete, reducing the silica modulus while increasing sodium hydroxide content enhances strength [68]. However, excessive alkali concentrations can accelerate dissolution during geopolymerization, ultimately leading to a decline in mechanical strength [69]. The results indicated that the abrasion resistance of porcelain-based geopolymer concrete decreased with increasing concentrations of sodium hydroxide (NaOH) in the activating solution. This reduction in durability is likely attributed to intensified alkali activation, which can lead to a more porous matrix and diminished cohesion under mechanical stress. Among the chemical exposure conditions tested, the most severe deterioration was observed in specimens immersed in 20% sulfuric acid (H_2SO_4), revealing a pronounced vulnerability to acidic environments. After 90 days of immersion, a substantial weight loss of 29.76% was recorded, underscoring the aggressive nature of sulfuric acid in degrading the geopolymer matrix. These findings highlight the critical importance of optimizing alkali concentration not only to enhance mechanical performance but also to ensure long-term durability, particularly in chemically aggressive settings. Further investigation into microstructural evolution, pore connectivity, and ion transport mechanisms could offer deeper insights into the degradation pathways and inform the development of more resilient geopolymer formulations.

Table 6. Rate of percentage in weight loss after chemical immersion

Rate of weight loss (% per day)				
$MgSO_4$				
Chemical immersion time (days)	**5%**	**10%**	**15%**	**20%**
3→7	0.018	0.031	0.049	0.047
7→14	0.020	0.027	0.027	0.033
14 →21	0.023	0.024	0.021	0.027
21→28	0.030	0.037	0.036	0.031
28→60	0.004	0.007	0.008	0.009
60→90	0.011	0.011	0.010	0.008
HCl				
3→7	0.070	0.071	0.082	0.231
7→14	0.050	0.127	0.161	0.124
14→21	0.157	0.154	0.203	0.301
21→28	0.154	0.305	0.399	0.455
28→60	0.088	0.107	0.125	0.166
60→90	0.100	0.111	0.136	0.168
H_2SO_4				
3→7	0.045	0.046	0.047	0.274
7→14	0.095	0.170	0.229	0.232
14→21	0.177	0.252	0.424	0.687
21→28	0.433	0.610	0.646	0.519
28→60	0.245	0.387	0.451	0.549
60→90	0.109	0.125	0.154	0.181

Table 7 presents a comparative overview of curing conditions for various low-calcium aluminosilicate precursors activated using a combination of sodium silicate and sodium hydroxide solutions. The results reveal distinct differences in thermal requirements and curing behavior among these materials. Fly ash Type F, known for its high reactivity, demonstrates effective solidification at relatively low curing temperatures—as low as 20 °C. This makes it well-suited for ambient curing environments and offers practical advantages such as reduced energy consumption in pre-cast production processes. In contrast, porcelain-based geopolymer materials exhibit significantly lower reactivity, requiring a minimum curing temperature of 60 °C to initiate the geopolymerization process. The dense microstructure and limited surface activity of porcelain particles necessitate additional thermal energy to activate the aluminosilicate network. Furthermore, porcelain-based geopolymer concrete typically demands extended curing durations (around 24 h) to achieve sufficient mechanical strength and long-term durability. Ground granulated blast-furnace slag (GGBFS), by comparison, displays greater curing flexibility. Due to its higher calcium content and latent hydraulic properties, GGBFS can solidify effectively at room temperature without compromising structural integrity. This behavior enables rapid setting and strength development under mild thermal conditions, making GGBFS an efficient and energy-saving alternative in geopolymer applications.

Table 7. Difference curing condition research findings

Reference	Binder materials	Type of alkali activator solution	Molarity (M)	Curing condition
Gunasekara et al. [70]	Fly ash Type F	Na_2SiO_3 with NaOH liquid solution	15M	Curing at 20°C for 24h after that heat cured in a dry oven for 24 h at 80°C
Kupawade-patil et al. [71]	Fly ash Type F	Na_2SiO_3 with NaOH liquid solution	14M	Curing at 80°C for 72h
Noushini et al. [72]	Fly ash Type F and Slag	Na_2SiO_3 with NaOH liquid solution	12M	Curing at 60°C 75°C 90°C for 8, 12, 18 and 24h
Pradhan et al. [73]	GGBFS	Na_2SiO_3 with NaOH liquid solution	10M-14M	Ambient cuing at room temperature
Experiment	Porcelain	Na_2SiO_3 with NaOH liquid solution	8M, 10M, 12M and 14M	Curing at 60°C 75°C 90°C and 105°C for 2 h for mortar and 24h for concrete

These findings underscore the critical role of precursor selection in determining optimal curing strategies for geopolymer systems. Fly ash Type F and ground granulated blast-furnace slag (GGBFS) offer advantages in low-temperature curing scenarios, whereas porcelain-based geopolymers require more controlled and elevated thermal environments to ensure successful activation and performance. Tailoring the curing regime to the specific material characteristics is essential for maximizing both efficiency and mechanical properties in geopolymer concrete. In this study, polycarboxylate was used as a superplasticizer (SP) to enhance the workability of fresh porcelain-based mixtures, added at a dosage of 0.5% by porcelain weight. Previous studies have shown that polycarboxylate SPs effectively reduce surface tension, thereby improving flowability [8, 12]. For comparison, a geopolymer concrete composed entirely of GGBFS was prepared using a sodium silicate-to-sodium hydroxide ratio of 2.5, a superplasticizer dosage of 2%, and a sodium hydroxide concentration of 12 M. The strength of porcelain-based geopolymer specimens was lower than that of GGBFS specimens. However, the GGBFS-based geopolymer also exhibited a slight decrease in strength under similar conditions [64].

The interaction between superplasticizer dosage and alkali concentration in geopolymer concrete (GPC) is complex, with optimal performance depending on the specific SP type and alkali source. High alkali concentrations, particularly above 14 M can render conventional SPs less effective or even detrimental [12]. Certain lignin-based or polycarboxylate ether (PCE)-based SPs have demonstrated better compatibility with specific alkali-activator systems [74]. While SPs generally improve workability, SPs may reduce compressive strength at higher dosages or under certain alkali conditions. Compatibility tends to be better in alkali activators containing Ca^{2}□ cations compared to conventional systems. Memon et al. [75] reported that SP dosages up to 5% were insufficient to achieve the required flowability for self-compacting geopolymer concrete. In contrast, dosages between 6% and 7% successfully produced the desired workability, with 7% yielding the highest compressive strength across all curing ages. Notably, when compared to porcelain-based mixtures, a 2% superplasticizer dosage led to a zero-slump condition and significantly prolonged the setting time. These observations highlight the importance of optimizing SP dosage and alkali concentration to balance workability, setting behavior, and mechanical performance in geopolymer systems.

5. Conclusions

This research investigated the shrinkages of porcelain-based geopolymer mortar and accelerated disintegration of porcelain-based geopolymer concrete by their exposure to acidic and alkaline environments. The deterioration was measured in terms of residual abrasive resistance weight loss. The summarized results were presented below:

- X-ray fluorescence (XRF) analysis revealed that the sanitary ware waste material used in this study is predominantly composed of silicon dioxide (SiO_2) and aluminum oxide (Al_2O_3), with levels of 55.97% and 18.23%, respectively. These oxides are essential components in geopolymer chemistry, as main oxides contribute to the formation of aluminosilicate gel networks during the geopolymerization process. The relatively high content of SiO_2 and Al_2O_3 suggests that the porcelain waste has strong potential as a precursor for geopolymer synthesis, particularly in low-calcium binder materials.
- The increasing of NaOH concentration increased early drying shrinkage and autogenous shrinkage. The highest shrinkage occurred for alkali-activated porcelain concrete produced by NaOH concentrations of 14 M, while the lowest shrinkage was found for the concentration of NaOH with 8 M. The peak time for drying shrinkage and autogenous shrinkage occurred at 7 hours after mixing. Whereas, early drying shrinkage and autogenous shrinkage were noticed at 2nd and 4th hours, respectively.
- An increase in alkali concentration was found to exacerbate early drying shrinkage in porcelain-based geopolymer systems. However, considering both the engineering requirements and the sustainable repurposing of sanitary ware waste, an alkali concentration of 14 M combined with an initial curing temperature of 105 °C is advisable for optimal activation and strength development. To counteract the adverse effects of high alkalinity on workability and shrinkage, a higher dosage of superplasticizer is necessary. This not only improves the flowability of the mix but also helps reduce shrinkage by enhancing particle dispersion and minimizing internal stress during the early stages of geopolymerization.
- The abrasion resistance of porcelain-based geopolymer concrete decreased with increasing NaOH concentrations. The greatest deterioration of the specimens was observed in 20% H_2SO_4. After 90 days of immersion, a weight loss of 29.76% was recorded.
- Among the chemical environments tested, specimens exposed to H_2SO_4 exhibited the highest degree of disintegration, indicating greater vulnerability to sulfuric acid attack compared to HCl and $MgSO_4$. At 20% concentration, the rate of deterioration was most pronounced in H_2SO_4, with a recorded loss of 0.687%, followed by HCl at 0.455%, and $MgSO_4$ at 0.031%. These results confirm that porcelain-based geopolymer concrete demonstrates lower corrosion resistance in H_2SO_4 environments relative to HCl and $MgSO_4$, emphasizing the need for careful consideration of exposure conditions in durability-focused applications.

6. Declarations

6.1. Author Contributions

Conceptualization, B.I.N.A.; methodology, B.I.N.A.; validation, B.I.N.A.; formal analysis, B.I.N.A.; investigation, R.A.; resources, B.I.N.A.; data curation, B.I.N.A.; writing—original draft preparation, B.I.N.A.; writing—review and editing, B.I.N.A. and R.A.; visualization, B.I.N.A.; supervision, B.I.N.A.; project administration, B.I.N.A.; funding acquisition, B.I.N.A. All authors have read and agreed to the published version of the manuscript

6.2. Data Availability Statement

The data presented in this study are available on request from the corresponding author.

6.3. Funding

Rajamangala University of Technology Thanyaburi (FRB67E0728), Grant Recipient: Borvorn Israngkura Na Ayudhya.

6.4. Acknowledgements

This research was supported by the National Science, Research and Innovation Fund, Thailand (TSRI), through Rajamangala University of Technology Thanyaburi (Project number: FRB67E0728). The authors would like to express our sincere gratitude to the TSRI for financial support for the project.

6.5. Conflicts of Interest

The authors declare no conflict of interest.

7. References

[1] Cuviella-Suárez, C., Colmenar-Santos, A., Borge-Diez, D., & Rosales-Asensio, E. (2019). Sanitary-ware factories: Heat recovery strategies to optimize energy and water consumption. Energy Procedia, 157, 719–736. doi:10.1016/j.egypro.2018.11.238.

[2] Fernandes, M., Sousa, A., & Dias, A. (2004). Environmental impact and emissions trade ceramic industry-A case study. Portuguese Association of Ceramic Industry APICER, Coimbra, Portugal.

[3] Cristiano, M. (2014). The use of ceramic waste aggregates in concrete: a literary review. Concrete 2014 Progetto E Tecnologia Per II Costruito, Termoli, Italy. doi:10.13140/2.1.2349.1846.

[4] García-Ten, F. J., Quereda Vázquez, M. F., Gil Albalat, C., Chumillas Villalba, D., Zaera, V., & Segura Mestre, M. C. (2016). Life Ceram. Zero waste in ceramic tile manufacture. Key Engineering Materials, 663, 23–33. doi:10.4028/www.scientific.net/KEM.663.23.

[5] Chindaprasirt, P., & Rattanasak, U. (2023). Calcium wastes as an additive for a low calcium fly ash geopolymer. Scientific Reports, 13(1), 16351. doi:10.1038/s41598-023-43586-w.

[6] Miller, S. A., Habert, G., Myers, R. J., & Harvey, J. T. (2021). Achieving net zero greenhouse gas emissions in the cement industry via value chain mitigation strategies. One Earth, 4(10), 1398–1411. doi:10.1016/j.oneear.2021.09.011.

[7] Mohaddes Khorassani, S., Siligardi, C., Mugoni, C., Pini, M., Cappucci, G. M., & Ferrari, A. M. (2020). Life cycle assessment of a ceramic glaze containing copper slags and its application on ceramic tile. International Journal of Applied Ceramic Technology, 17(1), 42–54. doi:10.1111/ijac.13382.

[8] Wongpattanawut, W., & Ayudhya, B. I. N. (2023). Effect of Curing Temperature on Mechanical Properties of Sanitary Ware Porcelain based Geopolymer Mortar. Civil Engineering Journal (Iran), 9(8), 1808–1827. doi:10.28991/CEJ-2023-09-08-01.

[9] Zuda, L., Bayer, P., Rovnaník, P., & Černý, R. (2008). Mechanical and hydric properties of alkali-activated aluminosilicate composite with electrical porcelain aggregates. Cement and Concrete Composites, 30(4), 266–273. doi:10.1016/j.cemconcomp.2007.11.003.

[10] Jang, H. S., & So, S. Y. (2015). The properties of cement-based mortar using different particle size of grinding waste insulator powder. Journal of Building Engineering, 3, 48–57. doi:10.1016/j.jobe.2015.06.007.

[11] Guerra, I., Vivar, I., Llamas, B., Juan, A., & Moran, J. (2009). Eco-efficient concretes: The effects of using recycled ceramic material from sanitary installations on the mechanical properties of concrete. Waste Management, 29(2), 643–646. doi:10.1016/j.wasman.2008.06.018.

[12] Wongpattanawut, W., & Ayudhya, B. I. N. (2024). Optimizing Alkali-Concentration on Fresh and Durability Properties of Defected Sanitary Ware Porcelain based Geopolymer Concrete. Civil Engineering Journal (Iran), 10(4), 1069–1092. doi:10.28991/CEJ-2024-010-04-05.

[13] Ramos, G. A., Pelisser, F., Paul Gleize, P. J., Bernardin, A. M., & Michel, M. D. (2018). Effect of porcelain tile polishing residue on geopolymer cement. Journal of Cleaner Production, 191, 297–303. doi:10.1016/j.jclepro.2018.04.236.

[14] Mangat, P., & Lambert, P. (2016). Sustainability of alkali-activated cementitious materials and geopolymers. Sustainability of construction materials. Woodhead Publishing, Sawston, United Kingdom. doi:10.1016/c2014-0-02849-3.

[15] Teixeira, O. G., Geraldo, R. H., da Silva, F. G., Gonçalves, J. P., & Camarini, G. (2019). Mortar type influence on mechanical performance of repaired reinforced concrete beams. Construction and Building Materials, 217, 372–383. doi:10.1016/j.conbuildmat.2019.05.035.

[16] Odeh, A., Al-Fakih, A., Alghannam, M., Al-Ainya, M., Khalid, H., Al-Shugaa, M. A., Thomas, B. S., & Aswin, M. (2024). Recent Progress in Geopolymer Concrete Technology: A Review. Iranian Journal of Science and Technology - Transactions of Civil Engineering, 48(5), 3285–3308. doi:10.1007/s40996-024-01391-z.

[17] Trincal, V., Multon, S., Benavent, V., Lahalle, H., Balsamo, B., Caron, A., Bucher, R., Diaz Caselles, L., & Cyr, M. (2022). Shrinkage mitigation of metakaolin-based geopolymer activated by sodium silicate solution. Cement and Concrete Research, 162, 106993. doi:10.1016/j.cemconres.2022.106993.

[18] Li, Z., Gao, P., & Ye, G. (2017). Experimental study on autogenous deformation of metakaolin based geopolymer. 2nd International RILEM/COST Conference on Early Age Cracking and Serviceability in Cement-Based Materials and Structures, 12-14 September, 2017, Brussels, Belgium.

[19] Archez, J., Farges, R., Gharzouni, A., & Rossignol, S. (2021). Influence of the geopolymer formulation on the endogeneous shrinkage. Construction and Building Materials, 298, 123813. doi:10.1016/j.conbuildmat.2021.123813.

[20] Lolli, F., Thomas, J. J., Kurtis, K. E., Cucinotta, F., & Masoero, E. (2021). Early age volume changes in metakaolin geopolymers: Insights from molecular simulations and experiments. Cement and Concrete Research, 144, 106428. doi:10.1016/j.cemconres.2021.106428.

[21] Ma, Y., & Ye, G. (2015). The shrinkage of alkali activated fly ash. Cement and Concrete Research, 68, 75–82. doi:10.1016/j.cemconres.2014.10.024.

[22] Panchmatia, P., Olvera, R., Genedy, M., Juenger, M. C. G., & van Oort, E. (2020). Shrinkage behavior of Portland and geopolymer cements at elevated temperature and pressure. Journal of Petroleum Science and Engineering, 195(5), 107884. doi:10.1016/j.petrol.2020.107884.

[23] Ridtirud, C., Chindaprasirt, P., & Pimraksa, K. (2011). Factors affecting the shrinkage of fly ash geopolymers. International Journal of Minerals, Metallurgy and Materials, 18(1), 100–104. doi:10.1007/s12613-011-0407-z.

[24] Kuenzel, C., Vandeperre, L. J., Donatello, S., Boccaccini, A. R., & Cheeseman, C. (2012). Ambient temperature drying shrinkage and cracking in metakaolin-based geopolymers. Journal of the American Ceramic Society, 95(10), 3270–3277. doi:10.1111/j.1551-2916.2012.05380.x.

[25] Yang, J., Wang, Q., & Zhou, Y. (2017). Influence of Curing Time on the Drying Shrinkage of Concretes with Different Binders and Water-to-Binder Ratios. Advances in Materials Science and Engineering, 2017, 1–10. doi:10.1155/2017/2695435.

[26] Xiang, J., Liu, L., Cui, X., He, Y., Zheng, G., & Shi, C. (2019). Effect of Fuller-fine sand on rheological, drying shrinkage, and microstructural properties of metakaolin-based geopolymer grouting materials. Cement and Concrete Composites, 104, 103381. doi:10.1016/j.cemconcomp.2019.103381.

[27] Olvera, R., Panchmatia, P., Juenger, M., Aldin, M., & van Oort, E. (2019). Long-term oil well zonal isolation control using geopolymers: An analysis of shrinkage behavior. SPE/IADC Drilling Conference and Exhibition, 5-7 March, 2019, Hague, Netherlands.

[28] Yuan, Q., Huang, Y. Ling, Huang, T. Jie, Yao, H., & Wu, Q. Hong. (2022). Effect of activator on rheological properties of alkali-activated slag-fly ash pastes. Journal of Central South University, 29(1), 282–295. doi:10.1007/s11771-022-4913-0.

[29] Ye, H., Cartwright, C., Rajabipour, F., & Radlińska, A. (2017). Understanding the drying shrinkage performance of alkali-activated slag mortars. Cement and Concrete Composites, 76, 13–24. doi:10.1016/j.cemconcomp.2016.11.010.

[30] Mastali, M., Kinnunen, P., Dalvand, A., Mohammadi Firouz, R., & Illikainen, M. (2018). Drying shrinkage in alkali-activated binders – A critical review. Construction and Building Materials, 190, 533–550. doi:10.1016/j.conbuildmat.2018.09.125.

[31] Scherer, G. W. (1990). Theory of Drying. Journal of the American Ceramic Society, 73(1), 3–14. doi:10.1111/j.1151-2916.1990.tb05082.x.

[32] Steiner, L. R., Bernardin, A. M., & Pelisser, F. (2015). Effectiveness of ceramic tile polishing residues as supplementary cementitious materials for cement mortars. Sustainable Materials and Technologies, 4, 30–35. doi:10.1016/j.susmat.2015.05.001.

[33] Sun, Z., Cui, H., An, H., Tao, D., Xu, Y., Zhai, J., & Li, Q. (2013). Synthesis and thermal behavior of geopolymer-type material from waste ceramic. Construction and Building Materials, 49, 281–287. doi:10.1016/j.conbuildmat.2013.08.063.

[34] Reig, L., Tashima, M. M., Soriano, L., Borrachero, M. V., Monzó, J., & Payá, J. (2013). Alkaline activation of ceramic waste materials. Waste and Biomass Valorization, 4(4), 729–736. doi:10.1007/s12649-013-9197-z.

[35] Cartwright, C., Rajabipour, F., & Radlińska, A. (2015). Shrinkage Characteristics of Alkali-Activated Slag Cements. Journal of Materials in Civil Engineering, 27(7), 4014007. doi:10.1061/(asce)mt.1943-5533.0001058.

[36] EN 196-1:1994. (1994). Method of testing cement-Part1: Determination of strength. European Committee for Standardization (CEN), Brussels, Belgium.

[37] ASTM C 157/C157M-17. (2024). Standard Test Method for Length Change of Hardened Hydraulic-Cement Mortar and Concrete. ASTM International, Pennsylvania, United States. doi:10.1520/C0157_C0157M-17.

[38] ASTM C944M. (2017). Standard Test Method for Abrasion Resistance of Concrete or Mortar Surfaces by the Rotating-Cutter Method. ASTM International, Pennsylvania, United States. doi:10.1520/C0944-99.

[39] Bakharev, T. (2005). Resistance of geopolymer materials to acid attack. Cement and Concrete Research, 35(4), 658–670. doi:10.1016/j.cemconres.2004.06.005.

[40] Xie, Y., Lin, X., Ji, T., Liang, Y., & Pan, W. (2019). Comparison of corrosion resistance mechanism between ordinary Portland concrete and alkali-activated concrete subjected to biogenic sulfuric acid attack. Construction and Building Materials, 228, 117071. doi:10.1016/j.conbuildmat.2019.117071.

[41] Yan, D., Chen, S., Jin, J., Zhu, X., Wang, J., & Zeng, Q. (2021). Chemical-physical-mechanical stability of MKG mortars under sulfate attacks. Advances in Cement Research, 33(5), 224–238. doi:10.1680/jadcr.19.00094.

[42] Choi, S. J., Choi, J. I., Song, J. K., & Lee, B. Y. (2015). Rheological and mechanical properties of fiber-reinforced alkali-activated composite. Construction and Building Materials, 96, 112-118. doi:10.1016/j.conbuildmat.2015.07.182.

[43] Park, S., & Pour-Ghaz, M. (2018). What is the role of water in the geopolymerization of metakaolin? Construction and Building Materials, 182(10), 360–370. doi:10.1016/j.conbuildmat.2018.06.073.

[44] Douiri, H., Louati, S., Baklouti, S., Arous, M., & Fakhfakh, Z. (2014). Structural, thermal and dielectric properties of phosphoric acid-based geopolymers with different amounts of H3PO4. Materials Letters, 116, 9–12. doi:10.1016/j.matlet.2013.10.075.

[45] Xiao, L., Zhang, C., Zhang, H., & Jiang, Z. (2024). Internal Curing Effects of Slag on Properties and Microstructure of Ambient-Cured Fly Ash-Based Geopolymer Mortar. Buildings, 14(12), 3846. doi:10.3390/buildings14123846.

[46] Rashad, A. M. (2015). An investigation of high-volume fly ash concrete blended with slag subjected to elevated temperatures. Journal of Cleaner Production, 93, 47–55. doi:10.1016/j.jclepro.2015.01.031.

[47] Davidovits, J. (2021). Geopolymer Science and Global Warming. Geopolymer Institute, Saint-Quentin, France.

[48] Nath, P., & Sarker, P. K. (2014). Effect of GGBFS on setting, workability and early strength properties of fly ash geopolymer concrete cured in ambient condition. Construction and Building Materials, 66, 163–171. doi:10.1016/j.conbuildmat.2014.05.080.

[49] Klima, K. M., Schollbach, K., Brouwers, H. J. H., & Yu, Q. (2022). Thermal and fire resistance of Class F fly ash based geopolymers – A review. Construction and Building Materials, 323, 126529. doi:10.1016/j.conbuildmat.2022.126529.

[50] Duran Atiş, C., Bilim, C., Çelik, Ö., & Karahan, O. (2009). Influence of activator on the strength and drying shrinkage of alkali-activated slag mortar. Construction and Building Materials, 23(1), 548–555. doi:10.1016/j.conbuildmat.2007.10.011.

[51] Lee, N. K., Jang, J. G., & Lee, H. K. (2014). Shrinkage characteristics of alkali-activated fly ash/slag paste and mortar at early ages. Cement and Concrete Composites, 53, 239–248. doi:10.1016/j.cemconcomp.2014.07.007.

[52] Peng, H., Long, Z. L., & Yang, Y. W. (2025). Study on the drying shrinkage behavior and influencing factors of fly ash-based geopolymers under different humidity conditions. Construction and Building Materials, 473, 141041. doi:10.1016/j.conbuildmat.2025.141041.

[53] Lou, Y., Huang, M., Kang, S., Hu, M., Wu, W., & Chen, S. (2024). Study on basic performance and drying shrinkage of binary solid waste geopolymer prepared with recycled powders and slag. Case Studies in Construction Materials, 20. doi:10.1016/j.cscm.2024.e03195.

[54] Musikasiri, T. (2017). Factors affecting fresh and hardened properties of geopolymer concrete made with high calcium fly ash. Master thesis, King Mongkut's University of Technology Thonburi, Bangkok, Thailand.

[55] Ruengsillapanun, K., Udtaranakron, T., Pulngern, T., Tangchirapat, W., & Jaturapitakkul, C. (2021). Mechanical properties, shrinkage, and heat evolution of alkali activated fly ash concrete. Construction and Building Materials, 299, 123954. doi:10.1016/j.conbuildmat.2021.123954.

[56] Aydin, S., & Baradan, B. (2014). Effect of activator type and content on properties of alkali-activated slag mortars. Composites Part B: Engineering, 57, 166–172. doi:10.1016/j.compositesb.2013.10.001.

[57] Kumar, S., Kumar, R., & Mehrotra, S. P. (2010). Influence of granulated blast furnace slag on the reaction, structure and properties of fly ash based geopolymer. Journal of Materials Science, 45(3), 607–615. doi:10.1007/s10853-009-3934-5.

[58] Yan, G., Hu, J., Chen, M., Ma, Y., Huang, H., Zhang, Z., Wei, J., Shi, C., & Yu, Q. (2025). Performance evaluation of reinforced slag-fly ash-ceramic waste powders ternary geopolymer concrete under chloride ingress environment. Construction and Building Materials, 478, 141447. doi:10.1016/j.conbuildmat.2025.141447.

[59] Hanumananaik, M., & Subramaniam, K. V. L. (2023). Influence of Process Variables on Shrinkage in Low-Calcium Fly-Ash Geopolymers. Journal of Materials in Civil Engineering, 35(6), 1–10. doi:10.1061/jmcee7.mteng-14761.

[60] Hanumananaik, M., & Subramaniam, K. V. L. (2023). Shrinkage in low-calcium fly ash geopolymers for precast applications: Reaction product content and pore structure under drying conditions. Journal of Building Engineering, 78, 107583. doi:10.1016/j.jobe.2023.107583.

[61] Chen, W., Li, B., Wang, J., & Thom, N. (2021). Effects of alkali dosage and silicate modulus on autogenous shrinkage of alkali-activated slag cement paste. Cement and Concrete Research, 141, 106322. doi:10.1016/j.cemconres.2020.106322.

[62] Hu, X., Shi, C., Zhang, Z., & Hu, Z. (2019). Autogenous and drying shrinkage of alkali- activated slag mortars. Journal of the American Ceramic Society, 102(8), 4963-4975. doi:10.1111/jace.16349.

[63] Ballekere Kumarappa, D., Peethamparan, S., & Ngami, M. (2018). Autogenous shrinkage of alkali activated slag mortars: Basic mechanisms and mitigation methods. Cement and Concrete Research, 109, 1–9. doi:10.1016/j.cemconres.2018.04.004.

[64] Liu, M., Wu, H., Yao, P., Wang, C., & Ma, Z. (2022). Microstructure and macro properties of sustainable alkali-activated fly ash mortar with various construction waste fines as binder replacement up to 100%. Cement and Concrete Composites, 134, 104733. doi:10.1016/j.cemconcomp.2022.104733.

[65] Jithendra, C., & Elavenil, S. (2019). Role of superplasticizer on GGBS based Geopolymer concrete under ambient curing. Materials Today: Proceedings, 18, 148–154. doi:10.1016/j.matpr.2019.06.288.

[66] Desole, M. P., Fedele, L., Gisario, A., & Barletta, M. (2024). Life Cycle Assessment (LCA) of ceramic sanitaryware: focus on the production process and analysis of scenario. International Journal of Environmental Science and Technology, 21(2), 1649–1670. doi:10.1007/s13762-023-05074-6.

[67] Kirschner, A., & Harmuth, H. (2004). Investigation of geopolymer binders with respect to their application for building materials. Ceramics-silikaty, 48(3), 117-120.

[68] Xie, Z., & Xi, Y. (2001). Hardening mechanisms of an alkaline-activated class F fly ash. Cement and Concrete Research, 31(9), 1245–1249. doi:10.1016/S0008-8846(01)00571-3.

[69] Lee, W. K. W., & Van Deventer, J. S. J. (2002). The effect of ionic contaminants on the early-age properties of alkali-activated fly ash-based cements. Cement and Concrete Research, 32(4), 577–584. doi:10.1016/S0008-8846(01)00724-4.

[70] Gunasekara, C., Law, D., Bhuiyan, S., Setunge, S., & Ward, L. (2019). Chloride induced corrosion in different fly ash based geopolymer concretes. Construction and Building Materials, 200, 502–513. doi:10.1016/j.conbuildmat.2018.12.168.

[71] Kupwade-Patil, K., & Allouche, E. N. (2013). Examination of Chloride-Induced Corrosion in Reinforced Geopolymer Concretes. Journal of Materials in Civil Engineering, 25(10), 1465–1476. doi:10.1061/(asce)mt.1943-5533.0000672.

[72] Noushini, A., Castel, A., Aldred, J., & Rawal, A. (2020). Chloride diffusion resistance and chloride binding capacity of fly ash-based geopolymer concrete. Cement and Concrete Composites, 105, 103290. doi:10.1016/j.cemconcomp.2019.04.006.

[73] Pradhan, P., Panda, S., Kumar Parhi, S., & Kumar Panigrahi, S. (2022). Factors affecting production and properties of self-compacting geopolymer concrete – A review. Construction and Building Materials, 344, 128174. doi:10.1016/j.conbuildmat.2022.128174.

[74] Pradhan, P., Panda, S., Kumar Parhi, S., & Kumar Panigrahi, S. (2022). Effect of critical parameters on the fresh properties of Self Compacting geopolymer concrete. Materials Today: Proceedings, 62(P12), 6325–6335. doi:10.1016/j.matpr.2022.02.506.

[75] Memon, F. A., Nuruddin, M. F., Demie, S., & Shafiq, N. (2012). Effect of superplasticizer and extra water on workability and compressive strength of self-compacting geopolymer concrete. Research Journal of Applied Sciences, Engineering and Technology, 4(5), 407–414.